J. Fluid Mech. (1969), *vol.* 35, *part* 4, *pp.* 737–757
Printed in Great Britain

The measurement of skin friction in turbulent boundary layers with adverse pressure gradients

By K. C. BROWN AND P. N. JOUBERT
Department of Mechanical Engineering, University of Melbourne

(Received 29 March 1968 and in revised form 22 July 1968)

This paper describes a floating-element skin friction meter which has been designed for use in adverse pressure gradients. The effects of secondary forces on the element, which arise from the pressure gradient, are examined in some detail. The limitations of various methods of measuring wall shear stress are discussed and the results from the floating element device are compared with measurements taken in a two-dimensional boundary layer using Preston tubes and velocity profiles. As it is planned to use the instrument later for direct measurements of the shear stress in three-dimensional boundary layers, the relevance of the instrument to this situation is also discussed.

1. Introduction

In their studies of three-dimensional turbulent boundary layers Perry & Joubert (1965), Smith (1965) and Joubert, Perry & Brown (1967) have questioned which component of the mean velocity vector, if any, should vary according to the familiar logarithmic 'law of the wall'. Since the resolution of this question necessitates accurate and reliable measurements of wall shear stress, an instrument utilizing the floating-element principle has been built with the intention of later making direct measurements in a strongly yawed three-dimensional turbulent boundary layer.

Inherent in the design of the device developed, however, are secondary forces, associated with the boundary-layer pressure gradient, which must be accounted for before reliable measurements can be made in a three-dimensional flow. These secondary forces have been examined in a simple two-dimensional situation by comparing the results obtained from the device with measurements of wall shear stress made by (i) Preston tubes and (ii) Clauser's method.

The present paper discusses the methods of skin friction measurement available, and describes the instrument which has been developed, its calibration, and the investigation of the secondary effects on the instrument of pressure gradients in two-dimensional flow.

2. Skin friction measurement techniques

The small size of the wall shear stress, when compared to the changes in pressure (normal stress) brought about by velocity changes, commonly gives

rise to great difficulty in the accurate measurement of skin friction in fluid flows. Typically wall shear stresses in the range 0–0·5 lb./ft.^{2} are associated with dynamic pressures, and therefore pressure changes, of the order of 50 lb./ft.^{2}, from which they must be separated. This has led to a great diversity among the techniques used and to the development of techniques suited only to particular situations. The diagram below may serve to classify the more important techniques, many of which have been reviewed in a similar context by Rechenberg (1963).

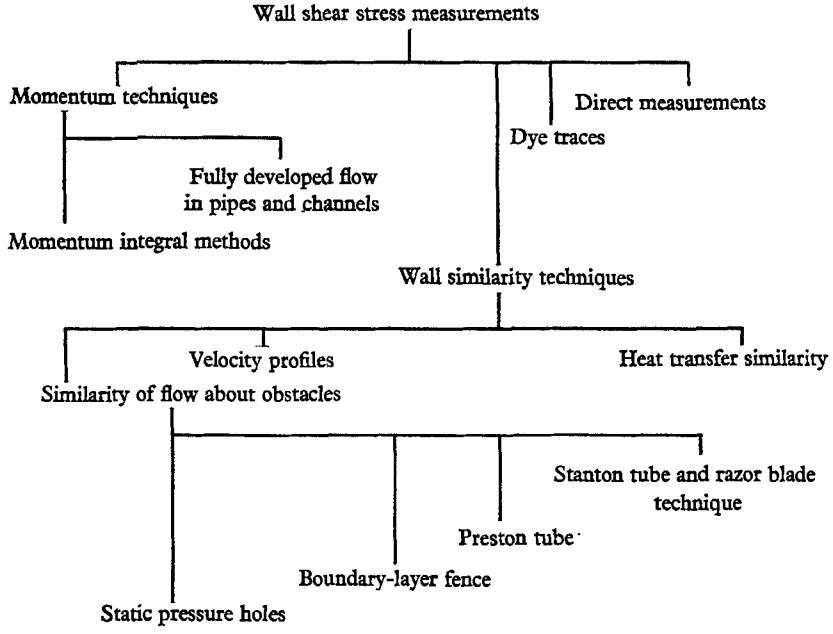

3. Momentum techniques

The better application of the momentum techniques is to fully developed flow in a straight parallel duct, where a simple momentum balance yields

$$\bar{\tau}_0 = W dp/dX,$$

where $\bar{\tau}_0$ is the mean of the wall shear stress τ_0 around the perimeter of the duct, W is the ratio of duct cross-sectional area to wetted perimeter and dp/dX is the streamwise pressure gradient in the duct. Two major difficulties have been encountered with the estimation of τ_0 from measurements of pressure loss dp/dX.

Firstly, Ferriss (1965) found that a very small streamwise taper of the duct is sufficient to cause large errors in the calculated wall shear stress due to the superposition of a contraction or diffusion pressure gradient upon the frictional pressure gradient. For example, a taper of 0·0004 in a 2 in. wide, two-dimensional channel, with a bulk velocity of 150 ft./sec, is sufficient to cause a 10 % error in the estimated τ_0. Secondly, although no circumferential changes in wall shear stress have been observed for fully developed pipe flow, it would seem advisable that their absence should be checked; Head & Rechenberg (1962)

found significant variations in the developing regions of a pipe. If adequate care is taken with the experiment, the method does provide a satisfactory reference for the calibration of shear stress measuring devices.

The application of the momentum principle to the problem of developing flow is less satisfactory. In principle, all that is required is to substitute measured quantities into the momentum integral equation appropriate to the type of boundary layer under consideration, and solve for τ_0. But experimentally determined quantities needed for developing flow include, as variables of major importance, derivatives of slowly varying quantities such as the momentum thickness of a boundary layer. Even with most careful velocity measurements it is difficult to accurately determine these derivatives. These inaccuracies are further accentuated in adverse pressure gradient boundary layers by the form of the momentum equations, so that the method proves particularly unsatisfactory as separation is approached. It has been shown by Clauser (1954) that three-dimensional effects may not be negligible in a nominally two-dimensional situation near separation, while Bidwell (1951) indicates that integral thicknesses formed from the Reynolds stresses should sometimes be included in the momentum equation. Thus for three-dimensional layers where strong pressure gradients exist near separation it is unlikely that this method would yield satisfactory results.

4. Wall similarity techniques

Near the wall in a turbulent two-dimensional flow the motion of the fluid can be said to be dominated by some 'wall variables'. That is, the influence of such variables as τ_0, kinematic viscosity ν, density ρ and distance from the wall Z is large, whilst others, the free-stream velocity u_1, for example, have no noticeable effect. This dominance is expressed in Prandtl's 'law of the wall',

$$\frac{u}{u_\tau} = \frac{u}{u_\tau}\left[\frac{Zu_\tau}{\nu}\right], \dagger \quad \text{where} \quad u_\tau = (\tau_0/\rho)^{\frac{1}{2}}. \tag{1}$$

This may be obtained by dimensional reasoning after assuming that the velocity u at a point near the wall depends upon the wall variables alone. This in turn leads to the concept that τ_0, which is one of the wall variables, can be found from measurements of the other variables provided that the form of the relationship has been previously determined.

Before discussing such techniques in detail, it is desirable to obtain an estimate of the distance from the wall Z_p at which the law of the wall starts to break down. A general result is not available, but the regional similarity approach to boundary-layer theory of Perry, Bell & Joubert (1966) and Perry (1966) can be used to give an estimate of the position of the first deviation of the velocity profile from the law of the wall, provided that this deviation is caused by an adverse pressure gradient (or one of its derivatives). According to this hypothesis the flow near the wall in a two-dimensional boundary layer with an adverse pressure

† Throughout this paper square brackets [ ] are used to denote a functional dependence.

gradient can be divided into at least three regions. In order from the wall they are:

$$\text{region I, the viscous sublayer} \quad \frac{u}{u_\tau} = \frac{Zu_\tau}{\nu}; \tag{2}$$

$$\text{region II, the logarithmic region} \quad \frac{u}{u_\tau} = \frac{1}{\kappa}\log_e\left(\frac{Zu_\tau}{\nu}\right) + A; \tag{3}$$

$$\text{region III, the half-power region} \quad \frac{u}{u_\tau} = K\left(\frac{\alpha Z}{u_\tau^2}\right)^{\frac{1}{2}} + \frac{\Delta u_1}{u_\tau}\left[\frac{\alpha\nu}{u_\tau^3}\right], \tag{4}$$

where κ, K and A are universal constants and α, following the notation of Perry & Joubert, is the kinematic pressure gradient $(1/\rho)\,dp/dX$. These three regions may not all be present at a given streamwise station in a boundary layer and are separated by small blending regions for which no equations have been deduced. It is clear that the 'law of the wall' extends as far as the outer edge of region II. Dimensional reasoning then indicates that, provided region III exists (i.e. provided that the first non-wall variable to enter the problem as Z is increased is the pressure gradient α), then

$$Z_p = Nu_\tau^2/\alpha, \tag{5}$$

since the fluid motion at this point is fully turbulent, making viscosity an unimportant variable in the consideration of mean motions. Perry *et al.* give the universal constant $N = 1{\cdot}41$ to represent the intersection of the logarithmic and half-power laws. This can be used for the present purposes, as experimental velocity profiles indicate that the blending region between regions II and III is thin.

If the logarithmic velocity distribution is assumed to start at $Zu_\tau/\nu = 30$, then it exists in the region $30\nu/u_\tau < Z < 1{\cdot}41u_\tau^2/\alpha$, and disappears entirely when $\alpha\nu/u_\tau^3 > 0{\cdot}05$. Thus the outer limit of the law of the wall is given by $Z_p = 1{\cdot}41u_\tau^2/\alpha$ provided that $\alpha\nu/u_\tau^3 < 0{\cdot}05$. For pressure gradients only slightly stronger than $\alpha\nu/u_\tau^3 = 0{\cdot}05$ the blending regions between regions I and II, and II and III, coalesce and no analytical deduction has been made, but, with much stronger pressure gradients (approaching separation), the half-power region can be considered to join to the viscous sublayer. Equivalent deductions may be made by a similar procedure. This extension to the theory will not be pursued here as the experimental data collected and reported later in this paper all have

$$\alpha\nu/u_\tau^3 < 0{\cdot}05.$$

(*a*) *Velocity profile methods*

By determining the function $(u/u_\tau)\,[Zu_\tau/\nu]$ in a situation such as a pipe or channel where wall shear stress is already known, u_τ can be estimated in any other situation from a measurement of the local velocity u at a point. Several variations of this method have been used, mostly with the object of ensuring that the points in the velocity profile that are being usedfor calc ulations are within the law of the wall. A successful method proposed by Clauser (1954) is based upon (3) rewritten in the form

$$\frac{u}{u_1} = \sqrt{\left(\frac{C_f'}{2}\right)}\left\{\frac{1}{\kappa}\log_e\left[\frac{Zu_1}{\nu}\sqrt{\left(\frac{C_f'}{2}\right)}\right] + A\right\},$$

when the local skin friction coefficient is defined by $C_f' = \tau_0/\frac{1}{2}\rho u_1^2$. This equation can be plotted in the form of a chart, figure 10, with C_f' as a parameter. When a velocity profile is plotted on the chart, the logarithmic portion can be readily seen and the appropriate value of C_f' read off by interpolation. Other approaches based on similar principles are to be found in papers by Bradshaw (1959) and Rajaratnam & Froelich (1967).

The linear sublayer (region I) can also be used for determining skin friction from the relationship $\tau_0 = \rho\nu\,\partial u/\partial Z|_{z=0}$, but the layer is so thin that accurate velocity measurements are difficult to obtain in this region.

(*b*) *Heat transfer similarity methods*

For boundary-layer flow along a surface the velocity field is independent of the temperature field provided that the temperature difference between surface and free stream $\Delta\theta$ is small (i.e. no natural convection). Conversely, however, the temperature field is not independent of the velocity field. Hence the rate of heat transfer Q by forced convection from a small heated element of surface of length l will depend on the wall variables if the thermal boundary layer above the element remains within the law of the wall; i.e.

$$Q = Q[C_p, l, k, \mu, \tau_0, \rho, \Delta\theta].$$

The new variables introduced here, C_p, k and μ, correspond to the specific heat at constant pressure, the thermal conductivity and the viscosity of the fluid respectively. At low speeds (small Eckert and Mach numbers) dimensional analysis gives

$$\frac{Q}{lk\Delta\theta} = \frac{Q}{lk\Delta\theta}\left[\frac{\mu C_p}{k}, \frac{lu_\tau}{\nu}\right].$$

For a given fluid the Prandtl number $\mu C_p/k$ is a constant, and this relationship may be further reduced to

$$Nu = Nu(R_\tau), \tag{6}$$

where the Nusselt number $Nu = Q/lk\Delta\theta$, and $R_\tau = lu_\tau/\nu$ can be interpreted as a friction Reynolds number.

Calibrating a given heated-element device in a known situation then allows τ_0 to be deduced from measurements of Q and $\Delta\theta$.

Heated-element devices were first introduced by Ludwieg (1949). They are generally constructed in the form of a small metal block, thin film or fine wire electrically heated and embedded in an insulating plug set flush with the surface. The temperature of the element is often determined from its resistance, whilst Q is taken as the electrical dissipation in the element, even though this will also contain the conduction and radiation heat losses.

Thin-film instruments developed by Bellhouse & Schultz (1964) and Brown (1967) are particularly useful as they are capable of detecting fluctuations in the wall shear stress, although to do this the thermal boundary layer should not only lie within the logarithmic region, but also remain entirely within the viscous sublayer. A similar restriction applies if the same calibration is to be used in both laminar and turbulent flow.

The use of fine wires was first suggested by Liepmann & Skinner (1954) and has since been used by Drinkuth & Pierce (1966) for the determination of skin friction direction; but general comments on the use of this technique, or other wall similarity techniques, in pressure gradients and skewed boundary layers are made later.

(c) *Similar flows about obstacles*

The velocity field about any small obstacle immersed entirely in the law-of-the-wall region† will be completely determined by the wall variables. The obstruction must, of course, be small enough to have a negligible effect upon the growth of the boundary layer in which it is placed. Thus any pressure difference

$$\Delta p = \Delta p[\tau_0, \rho, \nu, l],$$

and dimensional reasoning gives

$$\frac{\Delta p l^2}{\rho \nu^2} = \frac{\Delta p l^2}{\rho \nu^2}\left[\frac{\tau_0 l^2}{\rho \nu^2}\right]. \tag{7}$$

Again the form of the function may be established for any given obstacle say in a pipe flow, and thereafter a measurement of Δp is sufficient to determine τ_0. Furthermore, if the shape of the obstacle is such that other geometrically similar obstacles can be easily produced then the calibration of one device can be used for all similar devices. Several configurations have been used: the common ones are the boundary-layer fence (Head & Rechenberg 1962; Patel 1965); the Stanton tube (Fage & Falkner 1930) or the razor-blade technique (Wyatt & East 1966); a pair of static holes of different diameters (Duffy & Norbury 1967); and the Preston tube (Preston 1954). Although the razor-blade technique has met with some success only the Preston tube has a geometry reproduced with sufficient ease to enable the use of one calibration curve for all devices.

(d) *Applicability of wall similarity*

It is apparent that all of these devices rely upon the existence of wall similarity, and may therefore only be used in situations where the required law of the wall is known to exist. The existence of wall similarity in pipe flow has been demonstrated using data collected by Nikuradse (Schlichting 1962). Schultz-Grunow further demonstrated its existence in two-dimensional zero pressure gradient boundary layers. The case for a law of the wall in adverse pressure gradient boundary layers was first investigated by Ludwieg & Tillmann (1949) using a heat transfer device. Several other workers using Preston's technique have shown that tubes of differing size produce the same result for wall shear stress in a given situation. The repeatability of measurements with different wall similarity devices definitely indicates the existence of some form of wall similarity in an

† Good & Joubert (1968) reported that pressures on the front face of a two-dimensional fence depend only on the wall variables even when the fence height was much larger than the thickness of the law of the wall. However, this result may be peculiar to the two-dimensional, sharp-edged obstacle used, and could not be relied on for the design of a substantially three-dimensional obstacle used for measuring skin friction. In any case, a measuring device much larger than the thickness of the law-of-the-wall region would cause an unacceptable disturbance of the boundary layer.

adverse pressure gradient, although it may be argued that the correlating quantity u_τ has only been shown to equal $\sqrt{(\tau_0/\rho)}$ in pipes and zero pressure gradients when other reliable measurements of τ_0 are available. Certainly u_τ is an important correlating factor in the inner part of the boundary layer and we have no reason to suppose that its definition should be different in flow with and without a pressure gradient.

The problem of the law of the wall in three-dimensional or skewed turbulent boundary layers is, however, unresolved. The effect of the applied pressure gradient upon the mean velocity profile certainly extends deep into the wall region. This can be shown by integrating the equations of laminar motion after making the usual assumptions for flow very close to a smooth boundary. The result obtained when the pressure gradient is not neglected is

$$\frac{\mathbf{u}}{u_\tau} = \boldsymbol{\alpha}\frac{Z^2}{2\nu u_\tau} + \frac{Zu_\tau}{\nu}\hat{\mathbf{l}}, \tag{8}$$

where bold type indicates a vector quantity and $\hat{\mathbf{l}}$ the unit vector in the direction of the wall shear stress. Substitution of appropriate estimates of $\boldsymbol{\alpha}$ and u_τ into this equation for a typical velocity profile (Johnston 1957, station A-X5) indicates that the effect of the pressure gradient is not negligible, although the component in the direction of the wall shear stress is almost so. The curve shown in figure 1 as a solution to (8) was obtained by assuming a wall shear stress direction such that the curve obtained passed through the velocity profile points nearest to the origin (corresponding to $Zu_\tau/\nu \simeq 20$). This, in effect, gives an upper bound estimate of yaw angle; the actual yaw angle will be less in a turbulent boundary layer owing to the effect of the turbulent shear stress in the region. A better estimate can probably be obtained by assuming an appropriate eddy viscosity variation with Z, and a lower bound estimate of yaw angle is represented by the straight line from the origin to the first data point, as suggested by Johnston.

It is apparent, however, that the effects of a pressure gradient on a yawed boundary layer, or at least the component of the pressure gradient normal to the wall shear stress direction, cannot be neglected even at very small distances from the wall because of the yawing effect that it has on the velocity vector. Whether the law of the wall can be applied to a three-dimensional boundary layer is quite open to question and wall similarity techniques should, therefore, be avoided for quantitative measurements until more is known of the behaviour of the fluid near the wall in such a situation.

5. Dye traces

The use of dye in oil for surface flow visualization is well established. Meyer (1966) has shown further, not only that the placement of dye on the surface in discrete dots, instead of the usual painting, enhances the flow pattern obtained but also that the length of streak obtained from each dot correlates with the local wall shear stress. The method is not accurate enough for quantitative measurements but does provide much qualititative information, particularly regarding wall shear stress direction in complicated flows.

6. Direct measurements

The principle of measuring wall shear stress by cutting from the wall a small elemental piece, mounting it in such a way that it can move freely in the direction of the wall streamlines, and measuring the force on it, is quite straightforward. Furthermore, since no assumptions need to be made about the nature of the flow near the wall, the method appears satisfactory for measurements in a three-dimensional situation. It was used by early investigators such as Kempf (1929) for their studies of flat plate boundary layers in water. Schultz-Grunow (1940) and Smith & Walker (1959) have made successful measurements of the incompressible two-dimensional flat plate boundary layer in air, whilst Dhawan (1953),

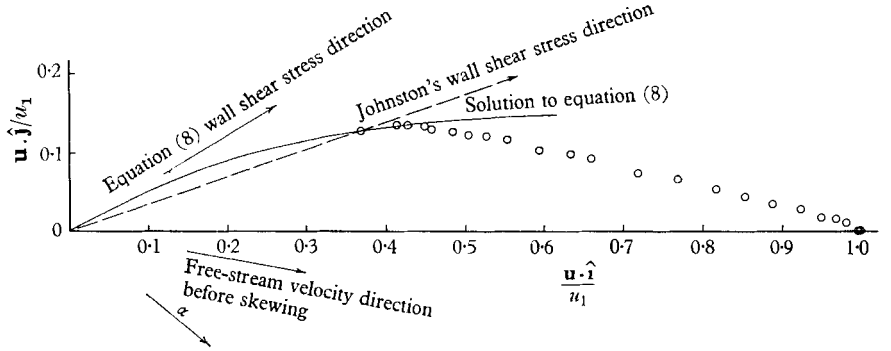

FIGURE 1. Hodograph of a three-dimensional velocity profile (Johnston 1957, station A-X5).

Hakkinen (1955), Coles (1953) and others have developed instruments for flat plates at high Mach numbers. However, secondary effects, associated mainly with the pressure gradient and the existence of an air gap around the element, have so far restricted the use of the floating element technique to zero pressure gradients. (The exceptions are Coles and Nalied & Thompson (1961), both of who have reported some tests in supersonic flow with very weak pressure gradients.)

The operating principle of a floating-element instrument is shown in figure 2, from which it is clear that the shear force on the element is simply the product of the shear stress τ_0 and the element area S, but to this shear force there should be added two other secondary forces: (i) a pressure force imposed on the edge of the element by penetration of the free-stream pressure into the air gap. If a pressure gradient exists, a net pressure or buoyancy force on the element in a direction opposing the pressure gradient results. Even if the width of the edge of the element is small, the effect of this pressure force F_p can be large at times, because the shear stress force approaches zero as separation is approached, whilst the pressure force does not. This direct pressure force can be estimated by assuming an effective edge width $C_1\epsilon$ over which the free-stream pressure is applied. (One would expect C_1 to be of order 0·5.) Then

$$\mathbf{F}_p = -C_1\epsilon\rho\alpha S.$$

As the direction of this force is not the same as the wall shear stress it may have a material effect upon the measured shear stress direction, even though the

pressure force is small compared with the shear stress force; (ii) the pressure gradient besides causing a direct pressure force on the element, will also cause a pressure difference between the boundary layer above any point in the air gap and the instrument case. (The case would presumably take up some mean pressure.) The resultant flow through the gap, presumably into the instrument on the high

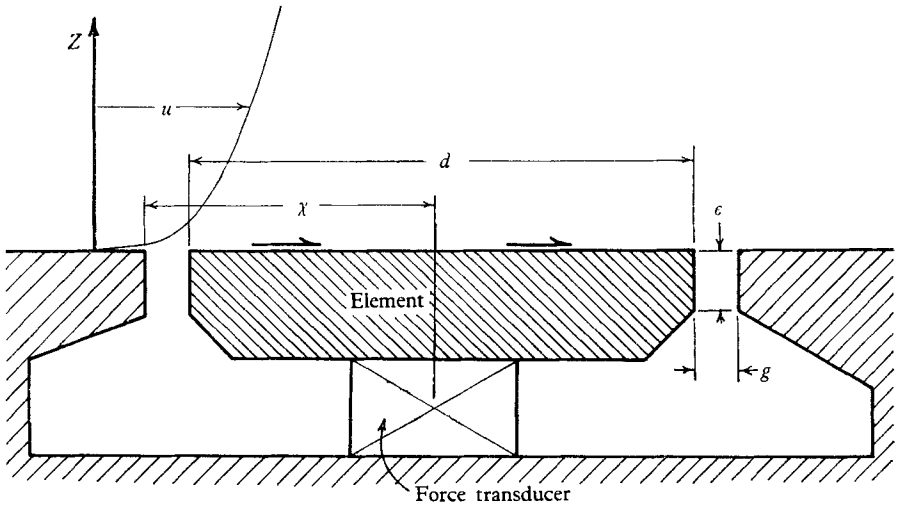

FIGURE 2. Floating-element shear stress meter principle.

pressure side and out from the case on the low pressure side, will result in a momentum exchange between the air in the instrument and the boundary layer. At least part of the force needed to maintain this momentum exchange will be transferred to the floating element. For small gap flows the direction of the force must be that of the wall shear stress, since that is the direction of fluid flow at the wall, although the force itself could be either positive or negative.

Treating the gap as an orifice, we may expect the volume flow rate through it to be proportional to $g\alpha^{\frac{1}{2}}S^{\frac{1}{4}}$, where g is the nominal width of the gap surrounding the floating element. We may also assume u_τ to be representative of the velocity near the wall so that the momentum exchange can be approximated by

$$\mathbf{F}_m = C_2 \rho g S^{\frac{3}{4}} \alpha^{\frac{1}{2}} u_\tau \hat{\mathbf{i}},$$

where C_2 is a constant of unknown magnitude.

A first approximation to the total force on the element is then given by

$$\frac{\mathbf{F}}{\tau_0 S} = \hat{\mathbf{i}} - C_1 \frac{\epsilon}{S^{\frac{1}{2}}} \frac{\alpha S^{\frac{1}{2}}}{u_\tau^2} + C_2 \hat{\mathbf{i}} \frac{g}{S^{\frac{1}{2}}} \frac{\alpha S^{\frac{1}{2}}}{u_\tau^2}. \tag{9}$$

Apart from these two additional secondary forces on the element, there are several less important effects which may be troublesome: (i) the air gap will act as a roughness element (groove) in a smooth plate, particularly if some misalignment is present between the element and its surroundings; (ii) even when the disturbance caused by the gap is ignored, there will still be a shear stress transmitted through the shear layer. Thus a part of the gap area should be

considered effectively element area as has been suggested by Hakkinen (1955); (iii) the shear stress measured is the mean shear stress over the area of the element. This would normally be unimportant for reasonably small devices but does set an upper limit on the size of instrument to be used where the wall shear stress is varying rapidly in the streamwise direction; (iv) the floating element, being free to move in the air gap, can alter the geometry of the device according to its position χ. A change in χ, say caused by a change in element force, will in turn result in changes in the flow pattern through the air gap with consequent changes in the momentum transfer forces.

Although these effects are difficult to account for in a detailed model, they may be easily included if a dimensional approach is used. The result is

$$\frac{F}{\tau_0 S} = \frac{F}{\tau_0 S}\left[\frac{S^{\frac{1}{2}}u_\tau}{\nu}, \frac{\alpha S^{\frac{1}{2}}}{u_\tau^2}, \frac{\chi}{S^{\frac{1}{2}}}\right], \tag{10}$$

where $S^{\frac{1}{2}}u_\tau/\nu$ and $\alpha S^{\frac{1}{2}}/u_\tau^2$ respectively represent a friction Reynolds number and an Euler number for the element. As this analysis makes use of a form of wall similarity it is important to point out that, owing to the inclusion of the pressure gradient α, it is a much more general similarity than is usually employed. Also it is only necessary to use the similarity for the consideration of secondary effects, which will be small for a well-designed instrument, and it in no way affects the validity of the measurement principle.

7. Description of the instrument developed

On the basis of the above discussion, it was decided to build a floating-element instrument for use in a three-dimensional situation. It is the only device which can be expected to give reasonable repeatability of results, and does not depend directly upon the absence of effects of pressure gradients for its operation.

Instruments of this type have been built using null reading force transducers. That is, the element force is balanced by an applied force (say a magnet or spring) so that the position of the element in the gap is constant. By using this technique it is conceivable that an instrument could be built with the air gap sufficiently small and well sealed to reduce gap flows to a negligible level, while the pressure forces could be completely balanced by suitable design. However, it was considered that the complexities of such a device would require a large amount of development work, so it was decided to build a simpler instrument, being careful to reduce secondary effects as much as possible. The secondary effects were studied by comparing measurements from the instrument with the results of wall similarity methods in a two-dimensional adverse pressure gradient boundary layer.

The general arrangement of the device, intended for use in the boundary layer on the upper surface of a horizontal flat plate, is shown in figure 3. The element has a nominal diameter of $\frac{3}{4}$ in. with a gap of 0·003 in. and an edge width of 0·0015 in. It is supported on three thin bronze leaf springs 1 in. in length and its position can be determined by means of a linear variable differential transformer. A viscous damper using 12,500 centistokes silicone lubricant is incorporated in the trans-

former mounting to reduce the effects of wind tunnel vibration; the resulting damping ratio is well above critical. Temperature variations in the low-speed wind tunnel did not require special consideration. Static pressure tappings are drilled in the face of the device and may be used to assist in the determination of

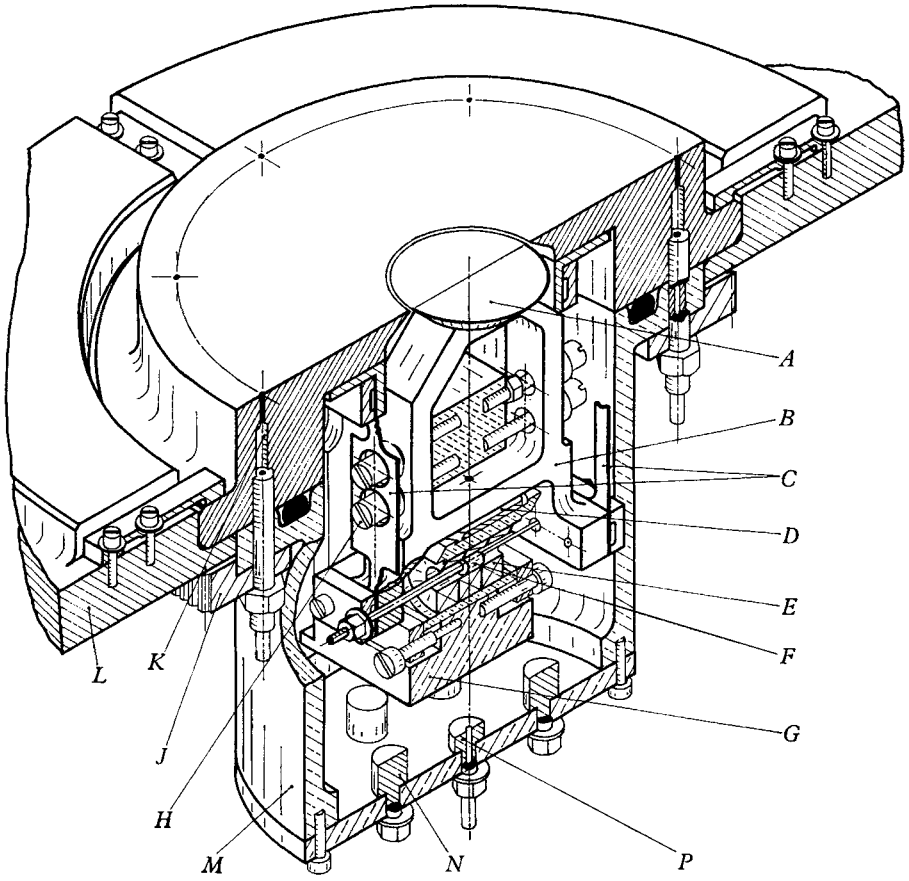

FIGURE 3. Arrangement of the floating-element shear stress meter. *A*, element; *B*, element support; *C*, leaf springs; *D*, damper plate; *E*, differential transformer; *F*, transformer core; *G*, transformer mount and slide; *H*, locking screws; *J*, gear; *K*, pressure tappings; *L*, instrument mounting plate; *M*, windshield; *N*, electrical terminals; *P*, pressure tapping.

the pressure gradient. The back of the device is covered with a sealed cylindrical windshield. The instrument has been equipped with an electric motor and gear train incorporated in the mounting so that it may be rotated about its vertical axis to find wall shear stress direction in a three-dimensional situation.

A selsyn is also fitted so that the angular orientation of the device can be read from outside the wind tunnel.

To ensure that the element was flush with the surrounding surface the face of the instrument was lapped flat after assembly. A check on the final alignment by means of a Talysurf showed that its mean position was correct but that a

variation up to 0·00055 in. existed at the circumference; the centreline average roughness of the element was 4 μin. and that of the surroundings 8 μin.

The supply to the differential transformer was from a 20,000 c/s sinusoidal oscillator, built for the purpose, which supplied the primary winding of the transformer with about 1 V r.m.s. A voltmeter was connected permanently across the primary winding to monitor the input. The output V_0, ranging from 0 to about 40 mV, was measured on a Flow Corporation r.m.s. voltmeter. The output was also monitored on an oscilloscope which was used to estimate the degree of mechanical vibration of the element superimposed upon the mean position signal.

8. Static calibration

Before use as a skin friction meter the stiffness of the element suspension was determined (i.e. the relationship between applied load and output voltage). This calibration was carried out by two separate leading methods: (i) the centre of a single strand of nylon fibre was attached to the element and the two ends

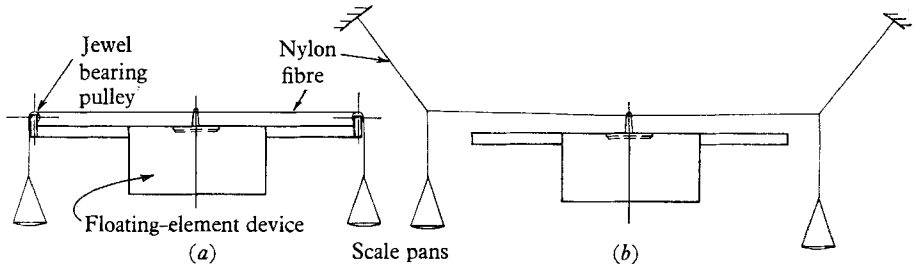

FIGURE 4. Calibration of the floating-element. (*a*) Pulley method. (*b*) Headley's method.

passed over two $\frac{3}{16}$ in. diameter aluminium pulleys mounted on jewelled bearings (see figure 4(*a*)). The ends were then tied to two miniature scale pans weighing approximately 85 mg each and the element was loaded by adding laboratory weights to the scale pans; (ii) for the second method, suggested by Headley (1966), 6 denier nylon fibres were used to suspend the scale pans as shown in figure 4(*b*). This method avoided the difficulties associated with imperfectly balanced pulleys and bearing friction, but introduced new variables: the angle between the fibres at the knot. These angles were found by photographing the knot under the applied load and measuring the angles on the negative by means of a surveyor's co-ordinatograph.

The two loading methods led to results in good agreement (0·1 % for stiffness) although more scatter existed in the results taken by the pulley method, probably due to bearing friction. The pulleys were used for most calibration purposes owing to their greater simplicity in use, and a typical calibration curve is shown in figure 5.

The determination of shear stress direction by the device is made possible by the suspension system used, which is sensitive only to the component of force in the direction of the differential transformer axis. The stiffness of the suspension

was determined with the load applied at various angles θ to the transformer axis, with the result shown in figure 6. The relationship is sinusoidal as required.

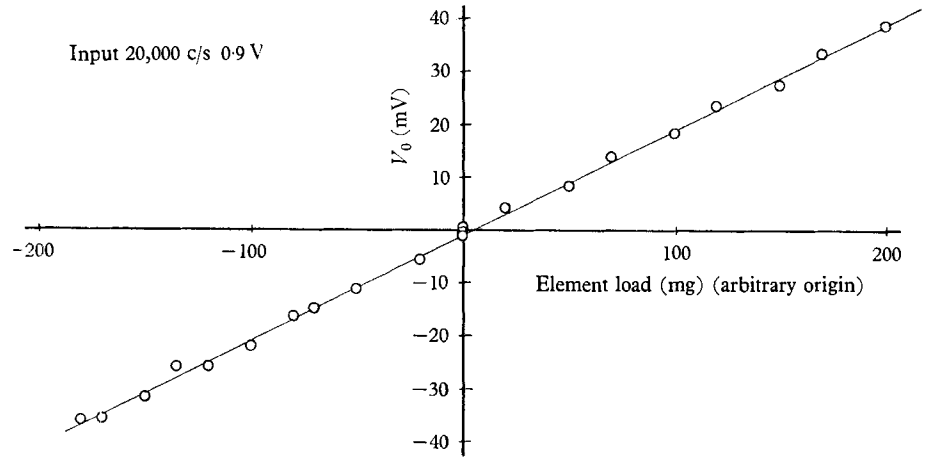

FIGURE 5. Typical calibration of the floating element.

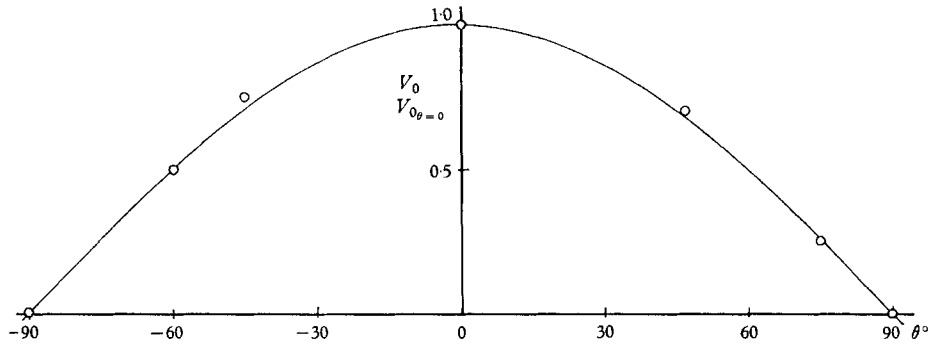

FIGURE 6. Relationship between floating-element output and loading direction.

9. Experimental investigation of secondary effects

As was indicated earlier in this paper the secondary effects on the floating-element device were investigated by comparing the results of element force measurements in a two-dimensional boundary layer in an adverse pressure gradient with wall shear stress measurements made by wall similarity methods. The object of this experiment was twofold: to find out how large the secondary effects were for the instrument devised and to obtain the information necessary to carry out a correction to floating-element results if one was necessary in a strong pressure gradient. Owing to the severity of the pressure gradients used, momentum methods were not considered.

10. Zero pressure gradient

The device was first placed in a nominally zero pressure gradient boundary layer where (9) indicates that the major secondary forces disappear and the wall shear stress on a circular element of diameter D is given by $\tau_0 = F/S$.

The instrument was mounted in the floor of a small wind tunnel with working section 13½ in. × 10 in., as shown in figure 7. A replacement for the device, in the form of a plug fitting in the same mounting and with provision for Preston tubes at the position of the centre of the element, was built and stainless-steel Preston tubes, 0·0362 in., 0·0290 in. and 0·0200 in. in diameter were fitted. Provision for taking mean velocity profiles using a static head tube, 0·040 in. diameter, fixed in the free stream and a flattened total head tube, frontal dimensions 0·0095 in. × 0·035 in., was made.

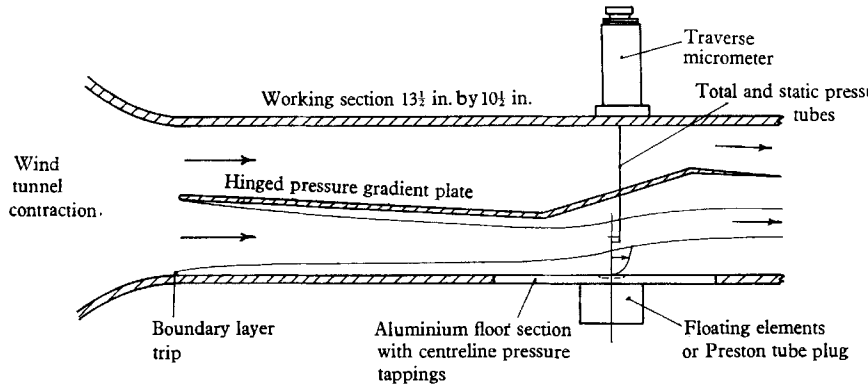

FIGURE 7. Wind tunnel working section.

Finally, a row of static pressure tappings were drilled on the centreline of the tunnel floor to facilitate the measurement of a pressure distribution imposed by a hinged plate located in the centre of the working section.

The variation of local skin friction coefficient with Reynolds number was first determined using Preston tubes. These tubes were also used to show that skin friction variations across the floor at the measuring station, and the effects of poor alignment of the instrument with the wind tunnel floor, were negligible. The calibration curve found by Patel (1965) was used in the Preston tube calibration. Local skin friction was also found from the velocity profiles by Clauser's method; the constants used in the logarithmic law of the wall were $\kappa = 0{\cdot}40$ and $A = 5{\cdot}1$.

Measurements of the force on the element then enabled calculation of τ_0 and C_f'. The element force, which ranged from 16×10^{-6} lb. to 440×10^{-6} lb., was always measured with the element in the same position in the air gap ($\chi/S^{\frac{1}{2}} =$ constant) whilst under load. This was achieved by tilting the instrument as a whole, raising the rear and depressing the front, until the element floated in the desired position with the load applied (the Preston tubes detected no change in wall shear stress due to the misalignment so caused). When the load was removed, by covering the face of the device with a celluloid bubble, the element moved to a different position, the displacement being due only to the removal of the element force. The fact that the element was not in its standard position when covered is immaterial since there was no fluid flow to cause secondary effects. By this method all readings from the floating element were taken with the wind tunnel running, minimizing such spurious effects as may have arisen from vibration of the work-

ing section and aerodynamic loads. A correction was applied to the output voltages to compensate for the differences between arithmetic mean positions and the r.m.s. position measured by the voltmeter. Readings where this correction exceeded 5 % of the output signal on a few occasions showed poor repeatability and were discarded.

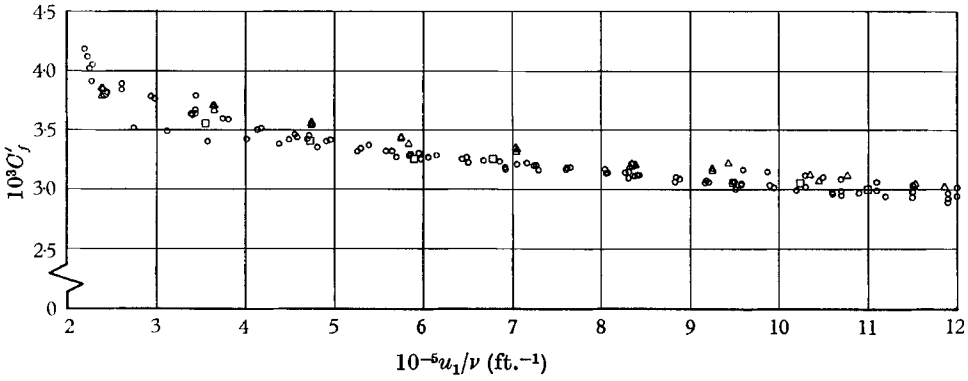

FIGURE 8. Skin friction in the nominally zero pressure gradient boundary layer. ○, Preston tube results; □, Clauser's method; △, floating-element results.

A comparison between the results of the three methods is shown in figure 8. The Preston tubes and Clauser's method are in good agreement, but the floating-element data are generally 4–5 % higher.

The discrepancy could be due to inaccuracy in the Preston tube calibration and the constants used in the logarithmic law of the wall. (For example, if the calibration of Preston tubes found by the Staff of the N.P.L. (1958) was used there would be much better agreement between the Preston tubes and the floating element.) However, Patel's calibration was considered the more reliable and the discrepancy has been attributed to slight secondary forces on the element. It will be seen from the model that the force due to pressure gradients is approximately proportional to $\alpha^{\frac{1}{2}}$ and will, therefore, be very sensitive to small pressure gradients. The slight misalignment of the element and the roughening effect of the gap are probably also contributory factors.

11. Adverse pressure gradients

Further tests were carried out in a variety of adverse pressure gradients, the pressure distribution being applied by means of the plate in the centre of the working section. By allowing the boundary layer to develop in a slightly favourable pressure gradient and applying the adverse pressure gradient by a steeply inclined portion of plate immediately above the measuring station, very strong adverse pressure gradients were obtained without separation or the inconvenience of very small wall shear stresses. This situation is also the two-dimensional equivalent of the suddenly yawed boundary layer on which measurements are to be made later.

(*a*) *Preston tubes in adverse pressure gradients*

Preston tubes and velocity profiles were again used to determine the skin friction coefficient over a range of Reynolds numbers for each pressure distribution. Patel's calibration of Preston tubes was also used but it was found that the tubes gave satisfactory results in much stronger pressure gradients than those indicated by Patel. The three tubes of different diameter in fact agreed with each other and with the velocity profile measurements in pressure gradients as high as $\alpha\nu/u_\tau^3 = 0{\cdot}023$ (the highest pressure gradient attained), whereas Patel gives a limit of $\alpha\nu/u_\tau^3 < 0{\cdot}015$ for operation within 6 % accuracy. The diameters of these tubes ranged from $du_\tau/\nu = 30$ to 50, and were well within Patel's prescribed limits of $du_\tau/\nu < 250$ for 6 % accuracy.

Thus it seems that Preston tubes can be used with higher values of $\alpha\nu/u_\tau^3$ without loss of accuracy provided that du_τ/ν is reduced. Patel's criterion does not take this into account.

The analysis based on regional similarity in the section on wall similarity techniques indicates that, if the first deviation from the law of the wall is caused by an adverse pressure gradient, and some logarithmic region exists ($\alpha\nu/u_\tau^3 < 0{\cdot}05$), then the important parameter is not $\alpha\nu/u_\tau^3$ but d/Z_p or $\alpha d/u_\tau^2$, where d is the Preston tube diameter. Furthermore, the first signs of failure should appear at about $d/Z_p = 1$ ($\alpha d/u_\tau^2 = 1{\cdot}41$). A short investigation was conducted in which Preston tubes of various sizes were all placed in a boundary layer at the same Reynolds number and pressure gradient. The wall shear stress was obtained by plotting the skin friction coefficient obtained from Patel's calibration against the Preston tube diameter and extrapolating to zero diameter. As was found by Patel the tube affected by the pressure gradient always overestimated the wall shear stress. The following limits upon the tube diameter for the indicated accuracies appear valid for adverse pressure gradient boundary-layer profiles with both a logarithmic region and a half-power region.

The existence of a logarithmic region makes it necessary to restrict the pressure gradient to $\alpha\nu/u_\tau^3 < 0{\cdot}05$ for this table to be valid, but unfortunately no similar criterion for the existence of a half-power region can be given.

Preston tube error (%)	$\alpha d/u_\tau^2$
1	1·34
2	1.74
3	2·06
5	2·55
7	2·98

These figures agree well with the value $\alpha d/u_\tau^2 = 1{\cdot}41$ predicted and appear to corroborate both the argument used here and the use of regional similarity in boundary-layer theory. The difference between this criterion and Patel's is demonstrated in figure 9. The agreement with Patel's 3 % error criterion is good but the present results indicate that Patel's 6 % limits are slightly optimistic at the outer limits of $\alpha\nu/u_\tau^3$ and du_τ/ν.

For completeness, representative velocity profiles taken at the measuring station are shown on Clauser's chart in figure 10 and correlated with the half-power equation in figure 11. It appears that the above criterion for Preston tube size can be applied in the present tests to those pressure gradients above $\alpha/u_\tau^2 \simeq 150\,\text{ft.}^{-1}$, i.e. where half-power laws appear to exist. At lower pressure gradients an overestimate of the allowable tube diameter results and the application of the limits on du_τ/ν recommended by Patel would seem in order.

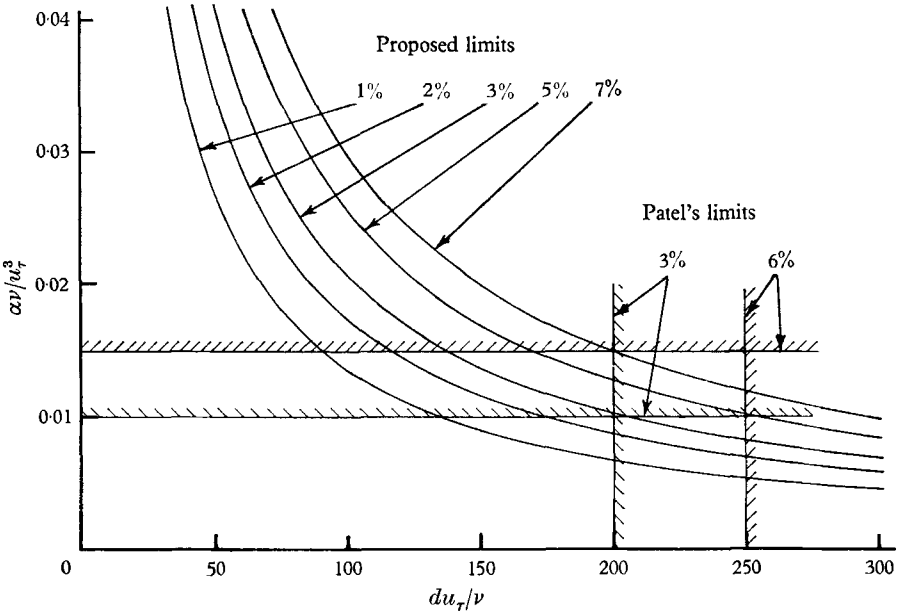

FIGURE 9. Preston tube error criteria.

(*b*) *The floating element in an adverse pressure gradient*

The results of element force measurements presented non-dimensionally in the form suggested by (10) are shown in figures 12 and 13. The wall shear stress used here was that found from the Preston tubes. It is clear that the secondary effects are relatively small (maximum 15 %) and that they do show a systematic trend. A multiple curvilinear regression surface of $F/\tau_0 S$ on $\alpha D/u_\tau^2$ and Du_τ/ν is also shown in the figures. If this surface was used to correct for the effects of secondary forces in the present data the standard deviation of $F/\tau_0 S$ would be 0·0272, giving a probability of 0·93 that an individual result would be within 5 % of the corresponding mean of Preston tube readings. This compares favourably with Preston tubes, which, in the present experiments, scattered over a range up to 10 % in width in the strongest pressure gradient.

(*c*) *Use of secondary force determinations for correction of three-dimensional flow measurements*

The above experiment represents a determination of the secondary forces in a two-dimensional flow. A similar investigation cannot be conducted in a three-dimensional flow because in such a situation the correct interpretation of the

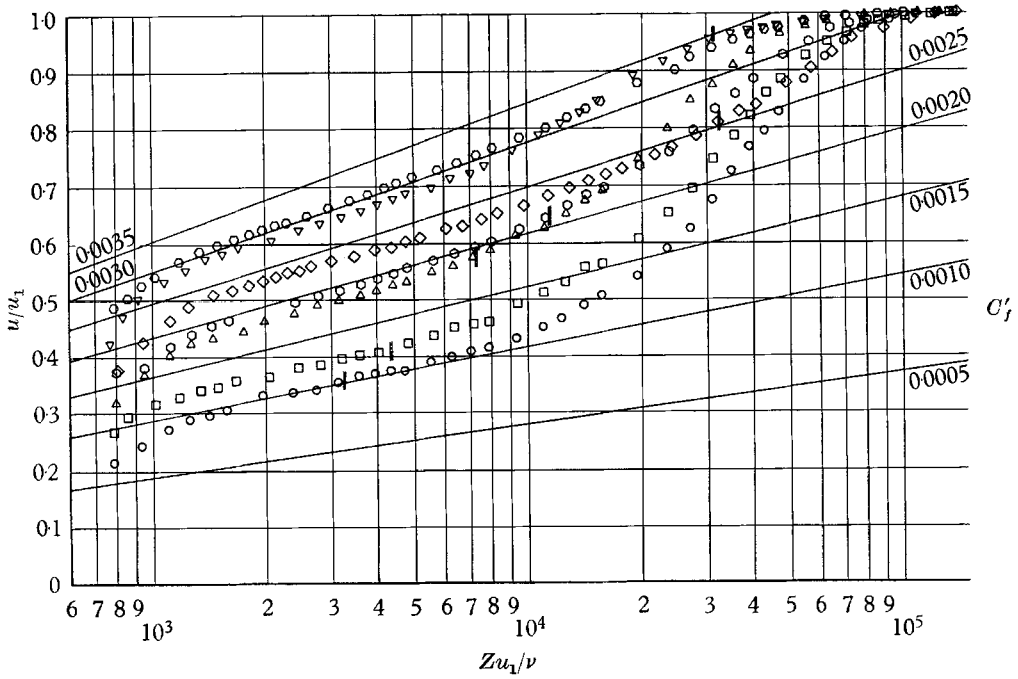

FIGURE 10. Typical velocity profiles on Clauser's chart. || indicates the theoretical junction of the logarithmic and half-power laws $Z_p = 1{\cdot}41u_\tau^2/\alpha$.

	○	▽	◇	⬡	△	□	○
α/u_τ^2 ft.$^{-1}$	−0·6	41.2	41.4	148	183	310	401
$10^{-5}\,u_1/\nu$ ft.$^{-1}$	9·48	9·25	9·70	9·66	9·49	9·41	9·32

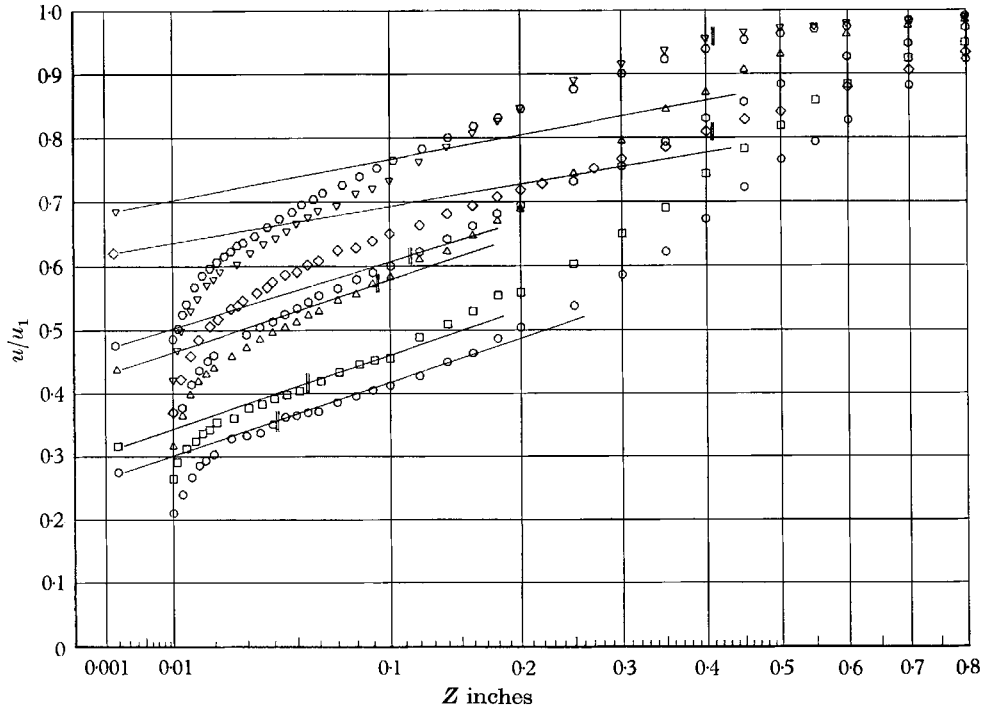

FIGURE 11. Typical velocity profiles correlated with the half-power law. || indicates the theoretical junction of the logarithmic and half-power laws $Z_p = 1{\cdot}41u_\tau^2/\alpha$. For values of u_1/ν and α/u_τ^2 see figure 10.

law of the wall is not known, and the wall similarity techniques used as an independent estimate of τ_0 with which to compare the floating-element instrument may not give reliable results. However, since the secondary forces involved are fairly small compared with the shear stress forces, it seems that any reasonable

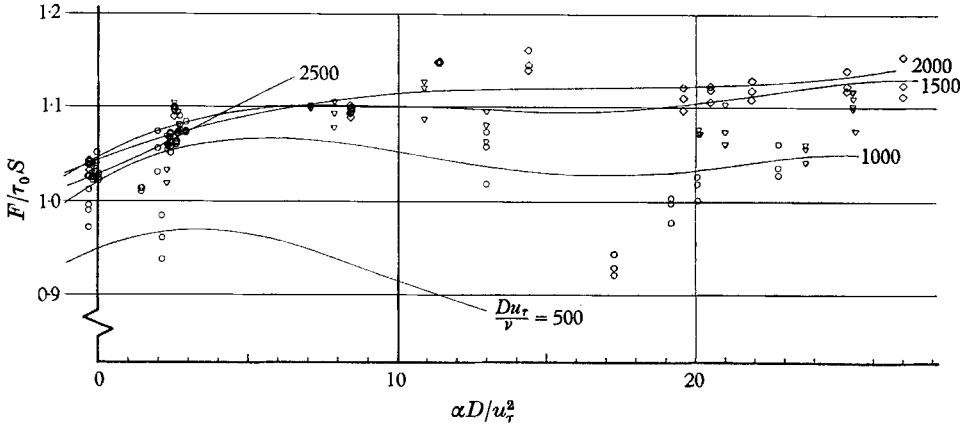

FIGURE 12. Secondary forces on the floating element in an adverse pressure gradient. ○, $500 < Du_\tau/\nu \leqslant 1000$; ▽, $1000 < Du_\tau/\nu \leqslant 1500$; ◇, $1500 < Du_\tau/\nu \leqslant 2000$; ⬡, $2000 < Du_\tau/\nu$.

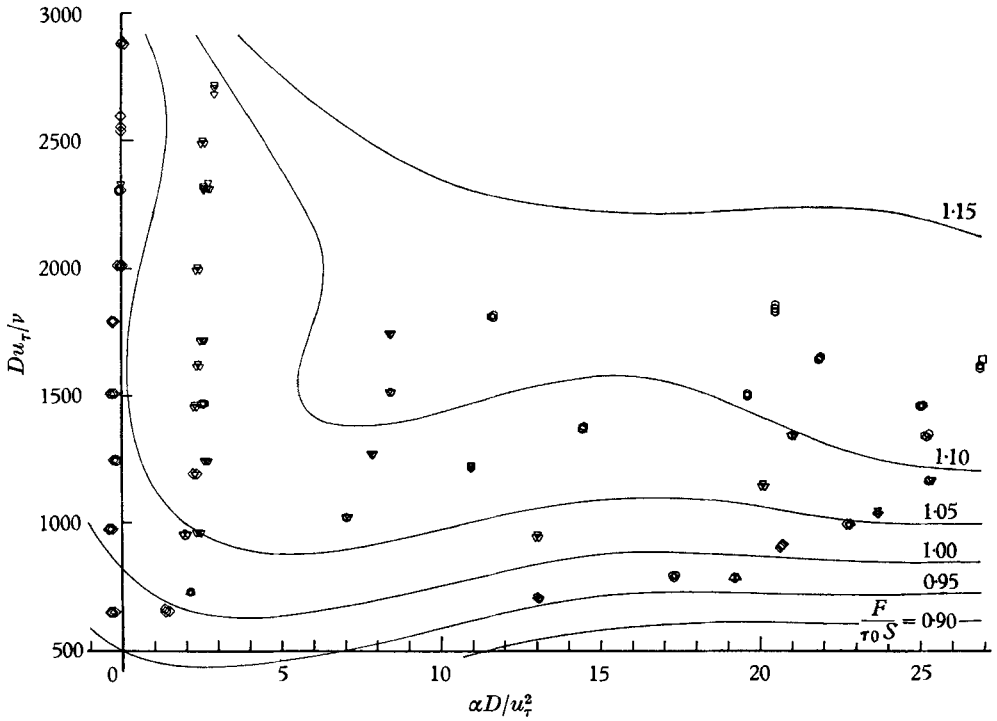

FIGURE 13. Contour plot of secondary forces. ○, $0{\cdot}9, < F/\tau_0 S \leqslant 0{\cdot}95$; △, $0{\cdot}95 < F/\tau_0 S \leqslant 1{\cdot}0$; ◇, $1{\cdot}0 < F/\tau_0 S \leqslant 1{\cdot}05$; ▽, $1{\cdot}05 < F/\tau_0 S \leqslant 1{\cdot}10$; ⬡, $1{\cdot}10 < F/\tau_0 S \leqslant 1.15$; □, $1{\cdot}15 < F/\tau_0 S$.

extension of the two-dimensional information into a three-dimensional situation will result in reasonably accurate final results.

From the previous discussion of the secondary effects, it seems that they can be divided into two groups: the direct effect of pressure gradient, resulting in a secondary force in the direction of the pressure gradient; and the other effects such as gap flows and roughness, all of which result in secondary forces in the direction of the wall streamlines. Furthermore, for the device in use, $\epsilon/D = 0{\cdot}002$, and, in the strongest pressure gradient used here ($\alpha D/u_\tau^2 = 28$), the maximum secondary force due to direct pressure gradient effects is only of the order of 3 % of the shear stress force. Most of the secondary force measured must be due to the indirect effects of pressure gradient, and the disturbance to the flow over the element.

It is proposed, therefore, that, in a three-dimensional boundary layer, a satisfactory estimate of secondary forces can be made by assuming that they are in the direction of the wall shear stress and are the same as in a two-dimensional situation with the same friction Reynolds number and element Euler number. The Euler number should be based upon the absolute value of the vector pressure gradient, as it is this which causes the flow through the air gap.

12. Conclusions

It has been found that in severe adverse pressure gradients the parameter $\alpha d/u_\tau^2$ forms a better criterion for the failure of Preston tubes than does the previously used $\alpha\nu/u_\tau^3$. Limits for $\alpha d/u_\tau^2$ are given as a guide to Preston tube accuracy.

The secondary forces on the element of a floating-element instrument due both to the direct effects of a pressure gradient, and to the distortion of the boundary-layer flow brought about by the air gap, have been investigated; the greatest secondary force found is 15 % of the wall shear stress force. The secondary force also shows some correlation with pressure gradient and Reynolds number so that corrections can be effected to shear stress measurements made by the instrument.

Because the secondary force component in the direction of the pressure gradient is much smaller than the component in the direction of the wall shear stress, the difference in these two directions can be ignored and the results of the two-dimensional study carried out here can also be applied to the estimation of secondary forces on the element when used in a three-dimensional situation.

The authors wish to acknowledge the assistance and encouragement received from Dr A. E. Perry during the course of this work.

REFERENCES

Bellhouse, B. J. & Schultz, D. L. 1964 *Aero. Res. Counc. R & M*, no. 3445.
Bidwell, J. M. 1951 *NACA TN* 2571.
Bradshaw, P. 1959 *J. Aero Space Sci.* **26**, 841.
Brown, G. L. 1967 *Heat Trans. Fluid Mech. Inst. Proc.*
Clauser, F. H. 1954 *J. Aero Sci.* **21**, 91.

COLES, D. 1953 Ph.D. Thesis, California Inst. of Tech.
DHAWAN, S. 1953 *NACA TR* 1121.
DRINKUTH, R. H. & PIERCE, F. J. 1966 *Rev. Sci. Instrum.* **37**, 740.
DUFFY, J. & NORBURY, J. F. 1967 *J. Roy. Aero Soc.* **71**, 55.
FAGE, A. & FALKNER, V. M. 1930 *Proc. Roy. Soc.* A **129**, 378.
FERRISS, D. H. 1965 *Aero. Res. Counc.* CP 831.
GOOD, M. C. & JOUBERT, P. N. 1968 *J. Fluid Mech.* **31**, 547.
HAKKINEN, R. J. 1955 *NACA TN* 3486.
HEADLEY, J. W. 1966 *AIAA J.* **4**, 1862.
HEAD, M. R. & RECHENBERG, I. 1962 *J. Fluid Mech.* **14**, 1.
JOHNSTON, J. P. 1957 *M.I.T. Gas Turbine Lab. Rep.* 39.
JOUBERT, P. N., PERRY, A. E. & BROWN, K. C. 1967 *Fluid Mechanics of Internal Flow*, Gino Sovran (ed.). Amsterdam: Elsevier.
KEMPF, G. 1929 *Werft, Reed. Hafen*, **10**, 234, 247.
LIEPMANN, H. W. & SKINNER, G. T. 1954 *NACA TN* 3268.
LUDWIEG, H. 1949 *Ing. Arch.* **17**, 207, also *NACA TM* 1284.
LUDWIEG, H. & TILLMANN, W. 1949 *Ing. Arch.* **17**, 288, also *NACA TM* 1285.
MEYER, R. F. 1966 *Nat. Res. Counc. Can. Rep.* LR-457.
NALEID, J. F. & THOMPSON, M. J. 1961 *J. Aero. Space Sci.* **28**, 940.
PATEL, V. C. 1965 *J. Fluid Mech.* **23**, 185.
PERRY, A. E. 1966 *J. Fluid Mech.* **26**, 481.
PERRY, A. E., BELL, J. B. & JOUBERT, P. N. 1966 *J. Fluid Mech.* **25**, 299.
PERRY, A. E. & JOUBERT, P. N. 1965 *J. Fluid Mech.* **22**, 285.
PRESTON, J. H. 1954 *J. Roy. Aero. Soc.* **58**, 109.
RAJARATNAM, N. & FROELICH, C. P. 1967 *J. Roy. Aero. Soc.* **71**, 52.
RECHENBERG, I. 1963 *Z. Flugwiss.* **11**, 429.
SCHULTZ-GRUNOW, F. 1940 *Luftfahrtforschung*, **17**, 239.
SCHLICHTING, H. 1962 *Boundary Layer Theory*, 4th ed. New York: McGraw-Hill.
SMITH, P. D. 1965 Ph.D. Thesis, Univ. of Lond.
SMITH, D. W. & WALKER, J. H. 1959 *NASA* R 26.
WYATT, L. A. & EAST, L. F. 1966 *RAE Tech. Rep.* 66027.